A molecular dynamics simulation study of the densities and viscosities of 1,2,4-trimethylbenzene and its binary mixture with n-decane

Xueming Yang [a,*], Qiang Liu [a], Xiaozhong Zhang [a], Chang Ji [a], Bingyang Cao [b,*]

[a] *Hebei Key Laboratory of Low Carbon and High Efficiency Power Generation Technology, Department of Power Engineering, North China Electric Power University, Baoding 071003, China*
[b] *Key Laboratory for Thermal Science and Power Engineering of Ministry of Education, Department of Engineering Mechanics, Tsinghua University, Beijing 100084, China*

ABSTRACT

N-decane and 1,2,4-trimethylbenzene (1,2,4-TMB) are components of many hydrocarbon aviation fuels and surrogate fuels. Obtaining and understanding their physical properties is crucial for their practical applications. In this study, the viscosities and densities of pure 1,2,4-TMB and its binary mixture with n-decane are investigated by equilibrium molecular dynamics (EMD) simulations with the COMPASS force field. The simulation results are compared with the predictions of several theoretical models: the modified Peng-Robinson (MPR) equation, Grunberg-Nissan (GN) model and UNIFAC-VISCO (UV) model for viscosity and the Peng-Robinson (PR) equation and the Tait equation for density, using NIST SUPERTRAPP data as a reference. Results show that the sixth-order mixing rules for MD simulations with the COMPASS force field provide a better prediction accuracy than the Lorentz-Berthelot mixing rules. The MD simulation results are in good agreement with the NIST SUPERTRAPP data, and the MD simulation model achieves better accuracy than the compared theoretical models. The self-diffusion coefficients of the components in the mixture are calculated and a comprehensive structural analysis is carried out to produce a better understanding of the effect of temperature on the viscosity and density of the binary mixture at a molecular level.

1. Introduction

Jet fuel is a complex mixture of many different aliphatic and aromatic hydrocarbons [1]. Its composition mainly consists of linear alkanes, branched alkanes, naphthenes, and aromatics. To study the properties of aviation fuels, surrogate fuels were widely used. Surrogate components are selected based on the components of jet fuels, which should represent the physical properties, chemical properties, or combustion properties of jet fuels [2]. Linear alkanes and aromatics have attracted wide attention due to their crucial roles as jet fuel constituents. The alkane compound N-decane and the aromatic compound 1,2,4-trimethylbenzene (1,2,4-TMB) are both included in many jet fuels, e.g., RP-3 and Jet A-1 aviation kerosene, and surrogate fuels [3–6]. Obtaining the thermophysical properties of fuel under sub/supercritical pressure is a prerequisite for the design and optimization of regenerative cooling systems and engine injection systems. While studying the combustion and ignition process of a given fuel, the flow characteristics in the nozzle should be taken as the foundation. Among many thermal properties,

viscosity is not only an important transport property but a basic parameter in the design and optimization of the jet engine [7]. Therefore, determining the thermophysical properties of fuels and surrogate fuels within a wide temperature and pressure range is necessary.

The experimental studies on the properties of aromatic hydrocarbons and their mixtures are still limited. Deng et al. [8] measured the densities and the residual molar volume of the 1,2,4-TMB and 2–methoxyethanol binary system at 298.15 K and 313.15 K at normal atmospheric pressure. Duan et al. [9] studied the spray spontaneous combustion characteristics of n-decane and several alkylbenzene blends in a heated constant volume spray combustor. The cetane number of the fuel mixture was measured in the temperature range of 808K-911 K, and both the ignition delay time and the combustion duration (varying with temperature) were measured. Duan et al. [10] measured the spray spontaneous combustion characteristics of two surrogate blends of RP-3 jet fuel with different proportions of n-decane and 1,2,4-TMB.

In recent years, molecular dynamics (MD) simulations have been widely used for studying the thermophysical properties of fuels [11–18]

Table 1
Group definition and non-bond parameters of the Lennard-Jones (9–6) potential for the COMPASS model [22].

Atom type	σ_{ij}(Å)	ε_{ij}/Kcal/mol	Definition
C_{H2}	3.854	0.062	Secondary sp3 carbon in linear alkyl chains
C_{H3}	3.854	0.062	Methyl group
C_a	3.9150	0.0680	Aromatic carbon

Table 2
Bond stretching parameters of COMPASS force field.

Atom type 1	Atom type 2	b_0	k_2	k_3	k_4
C_{H2}	C_{H2} or C_{H3}	1.53	299.67	−501.77	679.81
C_a	C_{H3}	1.501	321.90	−521.82	572.16
C_a	C_a	1.417	470.84	−627.62	1327.64
C_{H2} or C_{H3}	H	1.101	345.00	−691.89	844.60
C_a	H	1.0982	372.83	−803.45	894.32

Table 3
Bend stretching parameters of COMPASS force field.

Atom type 1	Atom type 2	Atom type 3	θ_0	k_2	k_3	k_4
C_{H2}	C_{H2}	C_{H2} or C_{H3}	112.67	39.52	−7.44	−9.56
C_a	C_a	C_{H3}	120.05	44.71	−22.74	0.00
C_a	C_a	C_a	118.90	61.02	−34.99	0.00
C_{H2} or C_{H3}	C_{H2} or C_{H3}	H	110.77	41.45	−10.60	5.13
H	C_{H2} or C_{H3}	H	107.66	39.64	−12.92	−2.43
C_a	C_{H3}	H	111.00	44.32	−9.45	0.00
C_a	C_a	H	117.94	35.16	−12.47	0.00

and other liquid organic mixtures [19]. Dianne et al. [11] used the molecular dynamics method to simulate the viscosities, densities and sound velocities of binary mixtures containing 1,2,4-TMB with 2,2,4, 6-pentamethylheptane in the temperature range of 253.15K-333.15 K under the pressure of 0.1 MPa. The results showed that the trend of variation of viscosity could not be predicted well by the OPLS-AA force field. Rabet et al. [12] studied the thermophysical characteristics of two biofuels 2,5-dimethylfuran (DMF) and 5-hydroxymethylfurfural (5-HMF) using MD simulations with the OPLS-AA, GAFF, and CHARMM27 force fields. The pure substances' liquid densities and vapor-liquid equilibria characteristics were computed and compared to the experimental data. Results showed that the GAFF model yields the best simulation accuracy for 2-methylfuran and DMF, while OPLS-AA is optimal for furfural. As reviewed in literatures [20,21], many studies have been conducted to investigate the thermodynamic and transport properties for n-alkanes; In general, transport property simulations for n-alkanes are sensitive to the force field employed. Hamani et al. [13] compared the TraPPE-UA force field model and the MCCG force field model in investigation of the thermophysical properties of binary mixtures of n-hexane and n-dodecane at temperatures ranging from 293.15 to 353.15 K and pressure up to 100 MPa. The results obtained by the TraPPE-UA force field yield an absolute average deviation (AAD) of 1.5% for the density and 35% for the viscosity. While the MCCG force field, it leads to slightly better results with an AAD of, 1.2% for the density, and 24% for the viscosity. Yang et al. [14] simulated the thermal conductivity of n-decane by the use of MD simulations, finding that the united-atom (UA) force field models show much better prediction accuracy than the all-atom force field models. Dysthe et al. [15] compared the viscosity of n-butane, n-decane, n-hexadecane, and 2-methylbutane under seven UA force fields. The results showed that the UA have large deviations in the prediction of viscosity, with the average absolute deviation as high as 80%. Furthermore, the longer the organic chain length, the greater the simulation deviation becomes. Yang et al. [16] compared the prediction of n-decane by five force fields using equilibrium molecular dynamics (EMD) simulations. They found that

the COMPASS force field combined with the Lorentz-Berthelot mixing rules exhibited the best accuracy for predicting the viscosity of n-decane with an average absolute deviation of 13.88% among the investigated UA and all-atom force fields. Payal et al. [18] used EMD method to calculate the shear viscosity of n-decane and n-hexadecane with force field models of the TraPPE-UA and the TTK-AA under ambient and high temperature-high pressure conditions. Their results showed that the shear viscosity derived from the UA force field is roughly 20% less than the experimental value, whereas the shear viscosity produced from the AA force field is around 10% higher.

In this study, the viscosities and densities of pure 1,2,4-TMB and its binary mixture with n-decane are investigated using molecular dynamics (MD) simulations with the COMPASS force field, and then compared with those by theoretical models. The self-diffusion coefficients of the components in the mixture are calculated and a comprehensive structural analysis is then carried out to produce a better understanding of the effect of temperature on the viscosity and density of the binary mixture of n-decane and 1,2,4-TMB with n-decane at a molecular level.

2. Methodology

2.1. Force field and potential

In MD simulations of this study, the COMPASS force field is adopted to simulate the viscosity and density of 1,2,4-TMB and its binary mixture with n-decane. The functional form of COMPASS force field is as follows [22]:

$$
\begin{aligned}
E_{total} &= E_b + E_\theta + E_\varphi + E_\chi + E_{b,b'} + \\
& E_{b,\theta} + E_{b,\varphi} + E_{\theta,\varphi} + E_{\theta,\theta,\varphi} + E_{elec} + E_{LJ} \\
&= \sum_b \left[k_2(b - b_o)^2 + k_3(b - b_o)^3 + k_4(b - b_o)^4 \right] + \\
& \sum_\theta \left[k_2(\theta - \theta_o)^2 + k_3(\theta - \theta_o)^3 + k_4(\theta - \theta_o)^4 \right] + \\
& \sum_\varphi [k_1(1 - \cos\varphi) + k_2(1 - \cos2\varphi) + k_3(1 - \cos3\varphi)] + \\
& \sum_\chi k_2\chi^2 + \sum_{b,b'} k(b - b_o)(b' - b'_o) + \sum_{b,\theta} k(b - b_o)(\theta - \theta_o) + \\
& \sum_{b,\varphi} (b - b_o)[k_1\cos\varphi + k_2\cos2\varphi + k_3\cos3\varphi] + \\
& \sum_{\theta,\varphi} (\theta - \theta_o)[k_1\cos\varphi + k_2\cos2\varphi + k_3\cos3\varphi] + \\
& \sum_{\theta,\theta,\varphi} k(\theta' - \theta'_o)(\theta - \theta_o)\cos\varphi + \\
& \sum_{i,j} \frac{q_i q_j}{r_{ij}} + \sum_{i,j} \varepsilon_{ij} \left[2\left(\frac{\sigma_{ij}}{r_{ij}}\right)^9 - 3\left(\frac{\sigma_{ij}}{r_{ij}}\right)^6 \right]
\end{aligned}
\tag{1}
$$

where E_b, E_θ, E_φ and E_χ are contributions of bond (*b*) stretching, angle (*θ*) bending, torsion angle (*φ*), and out-of-plane angle (*χ*), $E_{b,b'}$, $E_{b,\theta}$, $E_{b,\varphi}$, $E_{\theta,\varphi}$ and $E_{\theta,\theta,\varphi}$ are cross-coupling terms between internal coordinates, E_{elec} and E_{LJ} are non-bond interaction terms representing energy of the electrostatic Coulomb and van der Waals (VDW) term. b_o, θ_o and φ are equilibrium bond length, bond angle and torsion angle. k, k_1, k_2 and k_3 are force field-specific coefficients. In formula of E_{elec} and E_{LJ}, q_i is quantity of electric charge of an atom, r_{ij} is the distance between two atoms, ε_{ij} and σ_{ij} are the Lennard-Jones (LJ) potential interaction parameters, representing the energy parameter and the scale parameter, respectively. For the COMPASS model, the group definition and the non-bond parameters of the Lennard-Jones (9–6) potential are listed in Table 1.The COMPASS force field parameters for alkanes and aromatic hydrocarbons in this paper are taken from the Refs [22], as shown in

Table 4
Dihedral torsion parameters of COMPASS force field.

Atom type 1	Atom type 2	Atom type 3	Atom type 4	k_1	k_2	k_3
C_{H2}	C_{H2}	C_{H2}	C_{H2} or C_{H3}	0.0000	0.0514	−0.1430
C_{H3}	C_a	C_a	C_a	0.0000	4.4072	0.0000
C_a	C_a	C_a	C_a	8.3667	1.2000	0.0000
C_a	C_a	C_{H3}	H	−0.2802	−0.0678	−0.0122
C_{H2} or C_{H3}	C_{H2}	C_{H2} or C_{H3}	H	0.0000	0.0316	−0.1681
H	C_{H2}	C_{H2} or C_{H3}	H	−0.1432	0.0000	0.0617
C_a	C_a	C_a	H	0.0000	3.9661	0.0000
C_{H3}	C_a	C_a	C_{H3}	0.0000	4.5000	0.0000
C_{H3}	C_a	C_a	H	0.0000	1.5590	0.0000
H	C_a	C_a	H	0.0000	2.3500	0.0000

Tables 2–4.

2.2. Density

In this study, the density are calculated by the Eq. (4).

$$\rho = \frac{\sum NM}{VN_A} \tag{2}$$

where N is the atomic number; M is the molar mass; V is the volume of the simulation system; N_A is the Avogadro constant.

2.3. Viscosity

In this work, Green-Kubo formula [23] is used to calculate the shear viscosity, the expressions are as follows:

$$\eta = \frac{V}{K_B T} \int_0^\infty \left\langle \overrightarrow{P_{\alpha\beta}}(t) \cdot \overrightarrow{P_{\alpha\beta}}(0) \right\rangle dt \tag{3}$$

where V, K_B represent the volume of the system and the Boltzmann constant respectively, $\overrightarrow{P_{\alpha\beta}}(t)$ is the pressure tensor of time t, $\langle \overrightarrow{P_{\alpha\beta}}(t) \cdot \overrightarrow{P_{\alpha\beta}}(0) \rangle$ denotes the pressure-pressure tensor autocorrelation function (NACF), the pressure tensor formula is as follows:

$$\overrightarrow{P_{\alpha\beta}}(t) = \sum_i \overrightarrow{V_i} \overrightarrow{\varepsilon}_i + \frac{1}{2} \sum_{i,j,i\neq j} \overrightarrow{r_{ij}} \left(\overrightarrow{F_{ij}} \cdot \overrightarrow{v_{ij}} \right) \tag{4}$$

where $\overrightarrow{\varepsilon_i}$ is total energy including potential energy and kinetic energy, which can be expressed as $\overrightarrow{\varepsilon_i} = \frac{1}{2} m_i \overrightarrow{v_i}^2 + \frac{1}{2} \sum_{i\neq j} \phi(\overrightarrow{r_{ij}})$, $\phi(\overrightarrow{r_{ij}})$ denotes the potential energy between atom i and atom j. $\overrightarrow{v_i}$, $\overrightarrow{r_{ij}}$ represent the speed of the atom i and the distance between atoms situated at different positions respectively.

2.4. Molecular simulation details

All MD simulations are conducted using the Large-scale Atomic/Molecular Massively Parallel Simulator (LAMMPS) package [24]. The simulations are carried out in a three-dimensional cube box with periodic boundary conditions applied in the x-, y-, and z-directions. The initial size of the box is set to 50 Å × 50 Å × 50 Å. The simulation time step is set to 0.4fs. The velocity Verlet algorithm is used to integrate the Newton's equations. The long-range electrostatic interactions are computed with the particle-particle-particle-mesh (PPPM) method [25] with a cutoff distance of 14 Å and an accuracy of 10^{-4} in force. For LJ interactions, a cutoff distance of 14 Å is used. The adopted cut-off distance is sufficiently large (> 3.5σ, σ= 3.854 Å of C_{H2}) and consistent with the literature [26], offering a good balance of both the accuracy and efficiency of simulations. A long-range tail correction is applied for van der Waals interactions larger than the cut-off radius. The simulations initially run in the NPT ensemble with Nose-Hoover thermostat to control the pressure and temperature and to equilibrate the system at a given pressure and temperature for 1 ns. Then, there is a switch to the NVT ensemble with Nose-Hoover thermostat, used to equilibrate and relax the system at a given temperature for 1 ns. Another 1 ns is used to calculate the viscosity.

The strategies of the EMD simulations are adopted same as those in our previous studies [27]. We perform six independent simulations on pure fluid and mixtures by changing initial velocity to overcome the uncertainties for different independent runs of EMD simulations. The initial velocities are randomly assigned and obey a Gaussian distribution. In each independent run, a different seed number is used to generate unique initial velocity distributions under the same conditions. An average viscosity and density at the given temperature and pressure are evaluated by averaging over the values for the six independent runs, and the error estimate is obtained by the standard error of the values for each independent run.

The total number of molecules contained in all simulation systems is 400. For a system containing pure 1,2,4-TMB, the total number of molecules of 1,2,4-TMB is 400, corresponding to a total number of 8400 atoms. For the mixture containing 1,2,4-TMB and n-decane, 300 n-decane molecules and 100 1,2,4-TMB molecules are used; this corresponds to the surrogate model (75 mol% n-decane and 25 mol% 1, 2, 4-TMB) proposed by Liu et al. [3] for the RP-3 aviation kerosene. A previous study [16] by the authors has shown that the size of the system has a negligible effect on viscosity when the number of molecules exceeds 100, therefore, the number of molecules adopted in the present study is adequately high.

2.5. Theoretical calculation

2.5.1. Theoretical calculation of viscosity of the binary mixture

A theoretical model: the modified Peng-Robinson (MPR) equation of state [28,29], and two semi-theoretical models: Grunberg-Nissan (GN) model [30] and UNIFAC-VISCO (UV) model [31], are used for calculating the viscosity of binary mixture (n-decane and 1,2,4-TMB). These three models have been widely used for the viscosity calculation of hydrocarbons [29,32,33].

- MPR equation

The MPR equation is as follows [29]:

$$T = \frac{r_m P}{\eta_m - b'_m} - \frac{a_m}{\eta_m^2 + 2b_m \eta_m - b_m^2} \tag{5}$$

Rearranging Eq. (5) yields a cubic equation in mixture viscosity (η_m) for given pressure, temperature, and mixture composition, as illustrated in Eq. (6).

$$\eta_m^3 + \eta_m^2 \frac{(2b_m T - b'_m T - r_m P)}{T} + \eta_m \frac{(a_m - b_m^2 T - 2b_m b'_m T - 2r_m b_m P)}{T}$$
$$+ \frac{(b_m^2 b'_m T + r_m P b_m^2 - a_m b'_m)}{T}$$
$$= 0 \tag{6}$$

where the subscript m stands for mixing parameters. The parameters a_m and b_m are determined by implementing the linear mixing rule on a and b parameters of individual components, as well as their mole fraction, as shown in Eqs. (7) and (8); the parameter b'_m is evaluated by utilizing the quadratic mixing rule on b' and the mixture's mole fraction (Eq. (9)). The mole fraction of the ith component in the mixture is represented by x_i, where i and j are component indexes that range from 1 to N, with N denoting the number of components in the mixture.

Table 5
Group contributions for $G_{ij}(298)$.

group	Value of Δ_i
-C$_{H3}$	−0.100
>C$_{H2}$	0.096
Benzene ring	0.766

Table 6
All constants in the formula (36), (37), (38).

a	−9.070217	b	62.45326
d	−135.1102	f	4.79594
g	0.250047	h	1.14188
j	0.0861488	k	0.0344483

$$a_m = \sum_i x_i \frac{\Omega_a r_c^2 P_c^2}{T_c} \tag{7}$$

$$b_m = \sum_i x_i \frac{\Omega_b r_c P_c}{T_c} \tag{8}$$

$$b'_m = \sum_i \sum_j x_i x_j \sqrt{b_i b_j} \varphi (1 - k_{ij}) \tag{9}$$

$$r_m = \sum_i x_i \alpha \frac{T_c \mu_c}{Z_c P_c} \tag{10}$$

where Ω_a and Ω_b are constants in the formula, $\Omega_a = 0.457235529$, $\Omega_b = 0.077796074$. T_c, P_c, μ_c, and Z_c are critical temperature, critical pressure, critical viscosity and critical compression factor, respectively. k_{ij} is the binary interaction parameter. Due to the lack of experimental data, this paper defaults k_{ij} to be 0. Guo et al. [28] also proved that when k_{ij} is 0, the calculation results of alkane mixtures are credible. Parameters α and φ in Eqs. (9) and (10) respectively are given in Eqs. (11) and (12) below.

$$\alpha = \left(1 + K_1 \left((P_r T_r)^{0.5} - 1\right)\right)^{-2} \tag{11}$$
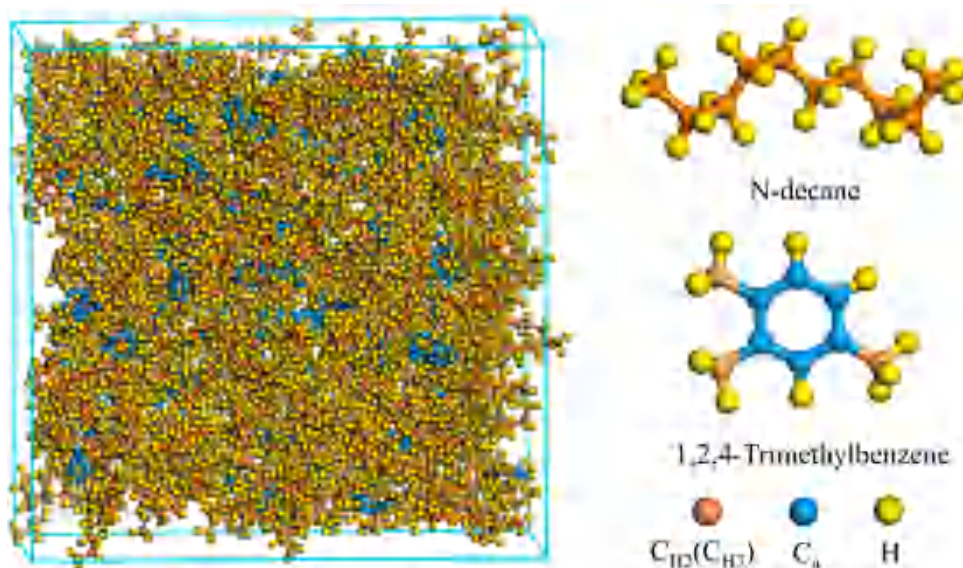
Fig. 1. Simulation system for mixtures of n-decane and 1,2,4-TMB with total molecular number $N = 400$.
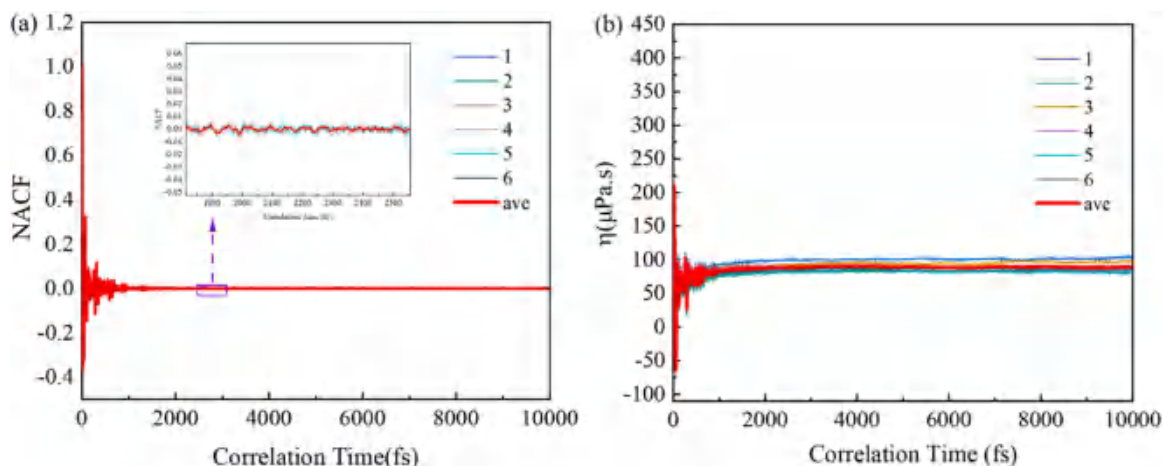
Fig. 2. The NACFs and calculated viscosities in six independent runs.
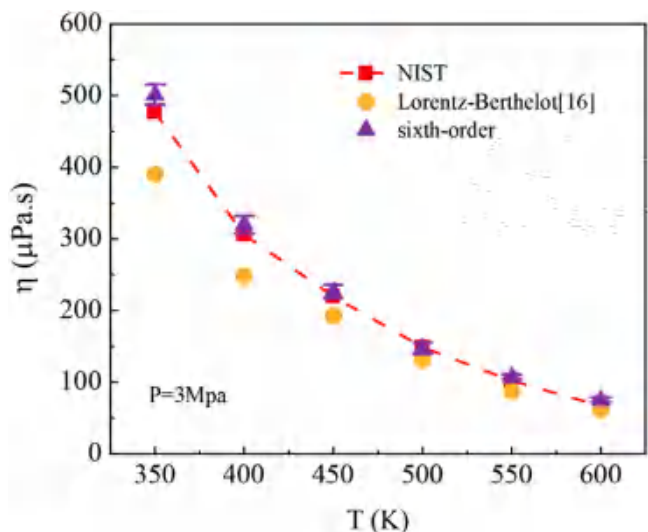
Fig. 3. Comparison of viscosity calculations of n-decane at $P = 3$ MPa using different combining rules.

$$\varphi = \exp\left(K_2\left(T_r^{0.5} - 1\right)\right) + \left(K_3\left(P_r^{0.5} - 1\right)^2\right) \tag{12}$$

where $T_r = T/T_c$ and $P_r = P/P_c$; T_r and P_r are the reduced temperature and pressure, the K_1, K_2 and K_3 describing n-alkanes are respectively given in Eqs. (13),(14) and (15), while those of describing aromatic

hydrocarbon are given in Eqs. (16),(17) and (18) below:

$$K_1 = 0.9744 + 0.3233\exp\left(-39.4521 C_N^{-0.9384}\right) \tag{13}$$

$$K_2 = 25.2955\exp(-0.2373 C_N) - 15.9920\exp(0.0032 C_N) \tag{14}$$

$$K_3 = -\frac{0.3291}{-0.1485 + \left(C_N^{-0.4550}\right)} \tag{15}$$

$$K_1 = 20.2060 - \frac{19.2573}{1 + \left(\frac{P_C}{0.2227}\right)^2} \tag{16}$$

$$K_2 = -\frac{1.1953 P_C}{-169.8919 + P_C} - \frac{13.1442 P_C}{-2.1857 + P_C} \tag{17}$$

$$K_3 = 0.3654\exp(0.0410 P_C) - 5538743.25\exp(-0.8635 P_C) \tag{18}$$

where K_1, K_2 and K_3 are component specific parameters dependent on the kind of component, C_N is number of carbons in the hydrocarbon, P_C above equations is critical pressure of the aromatic component.

- GN model

The formula of GN model is as follows [30]:

$$\ln\eta_m = x_1\ln\eta_1 + x_2\ln\eta_2 + x_1 x_2 G_{12} \tag{19}$$

where η_m and $\eta_i (i = 1, 2)$ are viscosity of mixture and pure component i, G_{ij} is an interacting parameter as a function of the components i and j as well as temperature shown in Eq. (20).
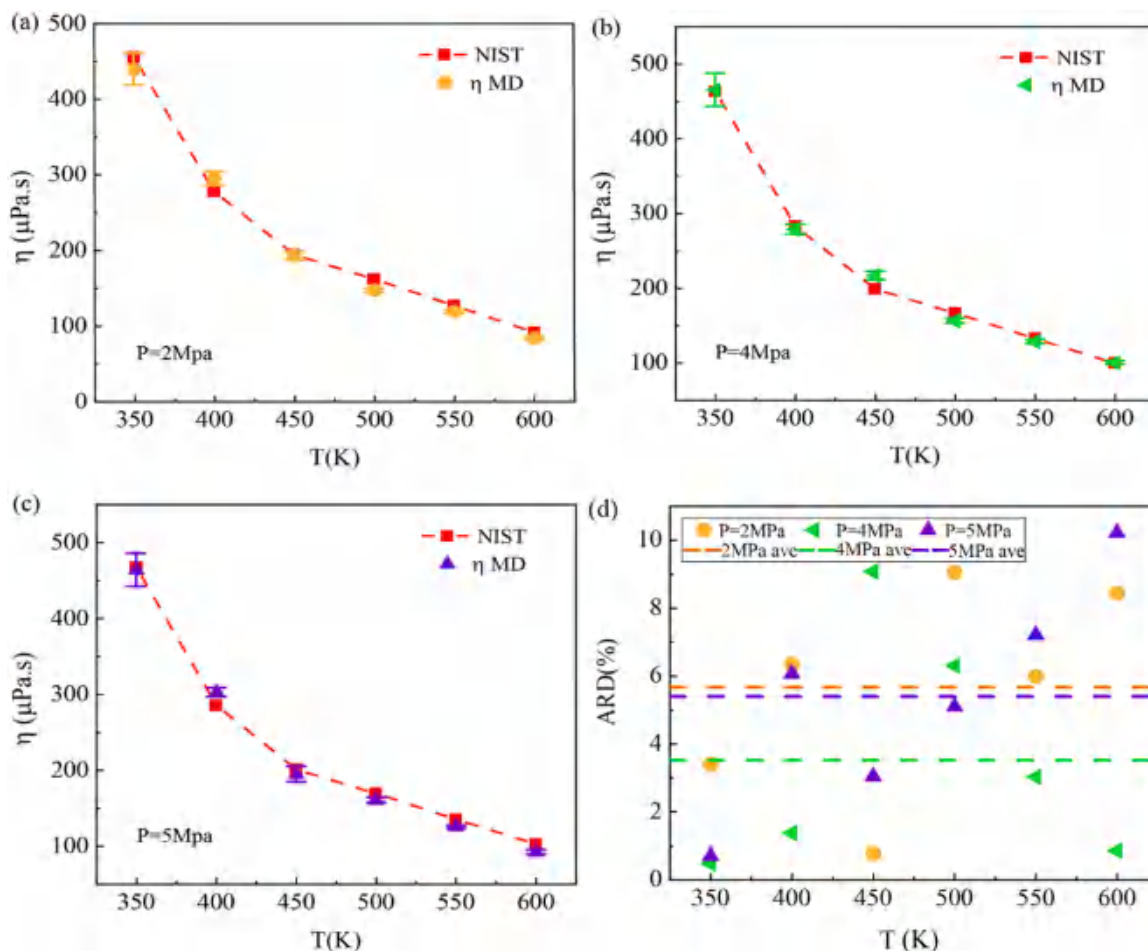
Fig. 4. Viscosity of 1,2,4-TMB as a function of temperature under different pressures: (a) 2 MPa; (b) 4 MPa; (c) 5 MPa; (d) ARDs and AARDs.
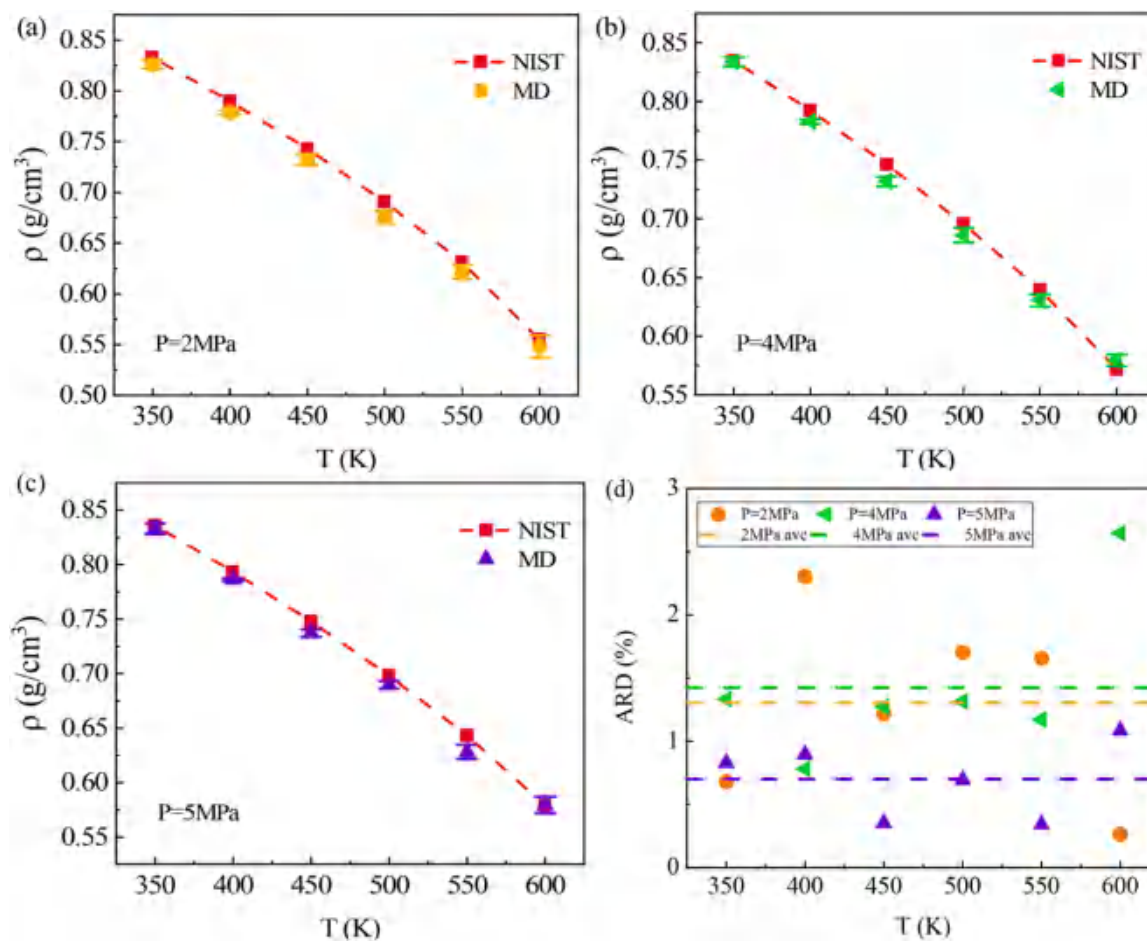
Fig. 5. Density of 1,2,4-TMB as a function of temperature under different pressures: (a) 2 MPa; (b) 4 MPa; (c) 5 MPa; (d) ARDs and AARDs.

$$G_{ij} = \sum \Delta_i - \sum \Delta_j + W \tag{20}$$

$$W = \frac{0.3161(N_i - N_j)^2}{N_i + N_j} - 0.1188(N_i - N_j) \tag{21}$$

The calculation of $\sum \Delta_i$ and $\sum \Delta_j$ can be obtained from the following Table 5. N_i and N_j are the number of carbon atoms in i, j molecules. If the components of mixture contain other types of atoms except carbon and hydrogen, $W = 0$. In addition, G_{ij} has a certain relationship with temperature for non-associated mixtures or associative mixtures, and the expression is as follows:

$$G_{ij}(T) = 1 - (1 - G_{ij}(298))\frac{573 - T}{275} \tag{22}$$

- UV model

The formula of UV model is as follows [31]:

$$\ln \eta_m = \sum_i x_i \ln(\eta_i v_i) - \ln v_m + \frac{\Delta * g^{EC}}{RT} + \frac{\Delta * g^{ER}}{RT} \tag{23}$$

where η_m is the viscosity of the mixture, x_i is the mole fraction, η_i is the viscosity of the pure component constituting the mixture, v_i and M_i is the molar volume and molar mass of the pure component, and v_m is the molar volume of the mixture, as shown in Eq. (24).

$$v_m = \frac{\sum_i x_i M_i}{\rho_m} \tag{24}$$

$\Delta * g^{EC}/RT$, $\Delta * g^{ER}/RT$ are the mixed terms, their calculation formulas are given in Eqs. (25) and (26).

$$\frac{\Delta * g^{EC}}{RT} = \sum_i x_i \ln\left(\frac{\phi_i}{x_i}\right) + \left(\frac{z}{2}\right)\sum_i q_i x_i \ln\left(\frac{\theta_i}{\phi_i}\right) \tag{25}$$

where ϕ_i is the molecular surface area fraction, θ_i is the molecular volume fraction, q_i is the van der Waals surface area of molecular i.

$$\frac{\Delta * g^{ER}}{RT} = -\sum\left(x_i \cdot \sum_k n_k^i \left[\ln \gamma_k^* - \ln \gamma_k^{*(i)}\right]\right) \tag{26}$$

where k is the index of group, n_k^i is the number of k groups in molecule i, γ_k^* and $\gamma_k^{*(i)}$ are the activity coefficient of group k in a mixture of groups in the actual mixture and formed from the groups in pure component i. The other parameters in Eq. (25) and Eq. (26) are provided in the supplementary material.

2.5.2. Theoretical calculation of density of binary mixture

Since PR equation [34] and Tait equation [35] are common models for calculating the density of organic matter, they are selected to calculate the density of binary mixtures of n-decane and 1,2,4-TMB.

PR equation

The PR equation is as follows [34]:

$$P = \frac{RT}{v_m - b_m} - \frac{a_m}{v_m(v_m + b_m) + b_m(v_m - b_m)} \tag{27}$$

Simplifying Eq. (27) produces a cubic equation in mixture's molar volume (v_m) for given pressure, temperature, and mixture composition,
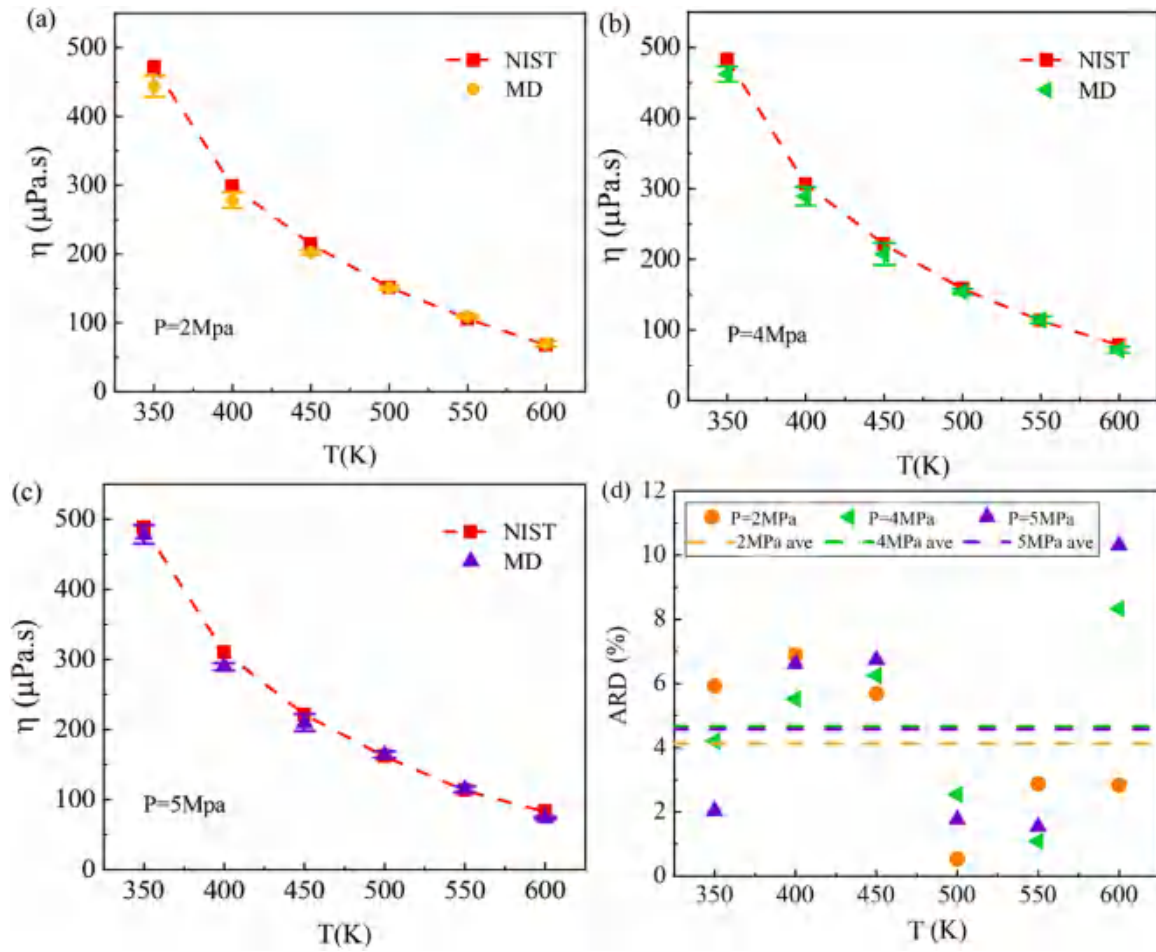
Fig. 6. Viscosity of the n-decane/1, 2, 4-TMB (75 mol% n-decane and 25 mol% 1, 2, 4-TMB) binary mixture as a function of temperature under different pressures: (a) 2 MPa; (b) 4 MPa; (c) 5 MPa; (d) ARDs and AARDs.

as illustrated in Eq. (28).

$$v_m^3 + v_m^2 \frac{(b_m P - RT)}{P} + v_m \frac{(a_m - 3b_m^2 P - 2Rb_m T)}{P} + \frac{(b_m^3 P + RTb_m^2 - a_m b_m)}{P} = 0$$

(28)

After getting the v_m of mixture, the ρ_m is calculated by Eq. (29).

$$\rho_m = M_m / v_m \tag{29}$$

In Eq. (28), a_m and b_m are state equation parameters, given in Eqs. (30) and (31), R is molar gas constant, v_m is molar volume.

$$a_m = \sum_i \sum_j x_i x_j \sqrt{a_i a_j} (1 - C_{ij}) \tag{30}$$

$$b_m = \sum_i \sum_j x_i x_j \sqrt{b_i b_j} (1 - D_{ij}) \tag{31}$$

where C_{ij} and D_{ij} are binary interaction parameters. Due to the lack of experimental data, the default values are 0. a_i and b_i defined in Eqs. (32) and (33) are the equation of state parameters for pure component i.

$$a_i = \frac{0.457535 \alpha_i(T) R^2 T_{ci}^2}{P_{ci}} \tag{32}$$

$$b_i = \frac{0.077796 R T_{ci}}{P_{ci}} \tag{33}$$

where $\alpha_i(T)$ expresses the temperature dependence in the parameter a_i

calculated by Eq. (34). T_{ci} and P_{ci} are critical temperature and pressure of pure component i.

$$\alpha_i(T) = \exp\left((2 + 0.836 T_{ri}) \left(1 - T_{ri}^{0.134 + 0.508 w_i - 0.0467 w_i^2} \right) \right) \tag{34}$$

where T_{ri} and w_i are the reduced temperature and acentric factor of pure component i.

Tait equation

The Tait equation is as follows [35]:

$$v_m = \frac{M_m}{\rho_m} = v_{s,m} \left(1 - c \ln \frac{\beta + P}{\beta + P_{s,m}} \right) \tag{35}$$

where v_m, ρ_m and M_m are molar volume, density and molar mass of mixture, $v_{s,m}$ and $P_{s,m}$ are the saturated molar volume and the saturated vapor pressure of mixture, the terms β and c are obtained from Eqs. (36) and (38).

$$\beta = P_{c,m} \left[-1 + a \left(1 - T_{r,m} \right)^{\frac{1}{3}} + b \left(1 - T_{r,m} \right)^{\frac{2}{3}} + d \left(1 - T_{r,m} \right) + e \left(1 - T_{r,m} \right)^{\frac{4}{3}} \right]$$

(36)

$$e = \exp\left(f + g w_{SRK,m} + h w_{SRK,m}^2 \right) \tag{37}$$

$$c = j + k w_{SRK,m} \tag{38}$$

where $w_{SRK,m}$ is the acentric factor, $T_{r,m}$ is the reduced temperature. The calculation formulas of $V_{s,m}$ and $P_{s,m}$ are provided in the supplementary material. All constants including $a - k$ except c and e in the formula are
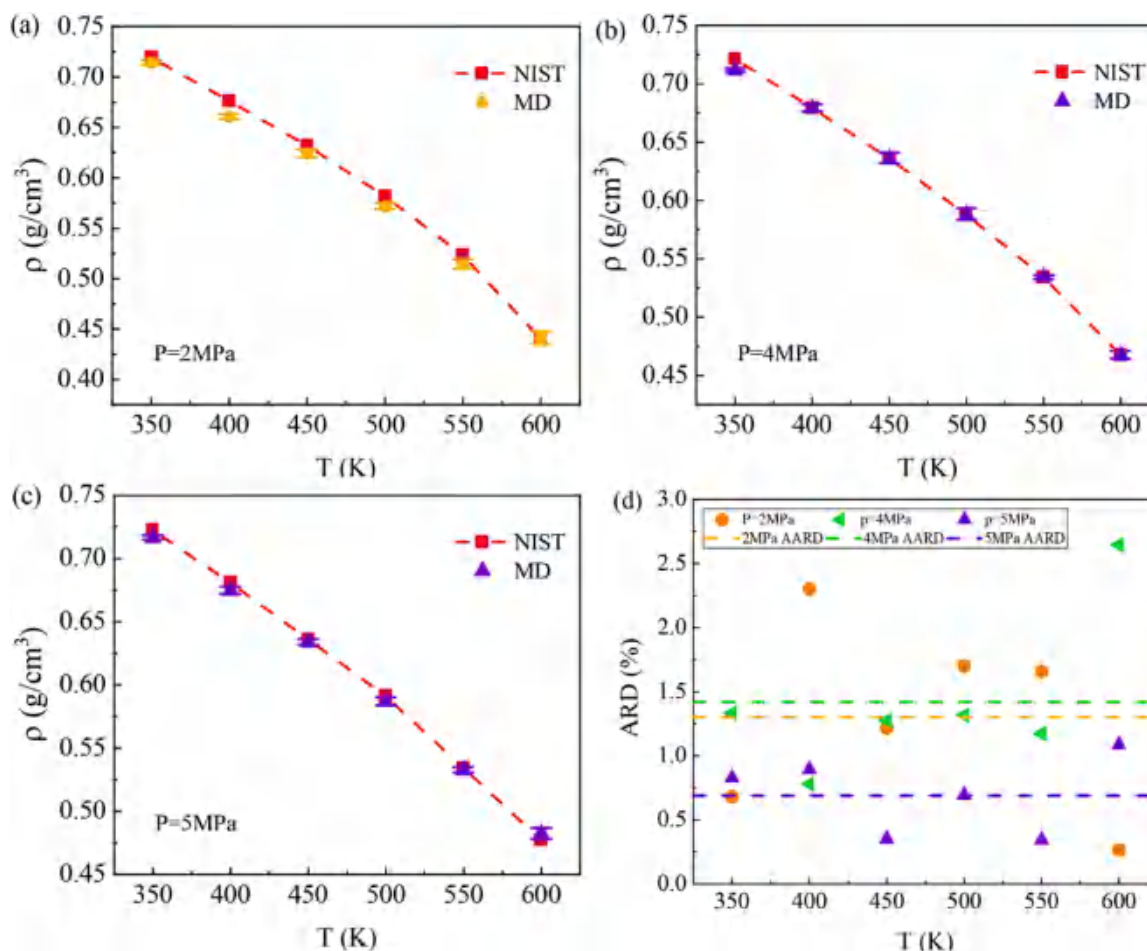
Fig. 7. Density of the n-decane/1, 2, 4-TMB (75 mol% n-decane and 25 mol% 1, 2, 4-TMB) binary mixture as a function of temperature under different pressures: (a) 2 MPa; (b) 4 MPa; (c) 5 MPa; (d) ARDs and AARDs.

shown in the following Table 6.

3. Results and discussion

The viscosities and densities of 1,2,4-TMB and its binary mixture with n-decane at temperatures of 350K-600 K and different pressures are calculated by MD simulations and theoretical models. Here data from the NIST SUPERTRAPP [36] are used as a reference. Many studies [37–39] have taken NIST SUPERTRAPP data of alkanes as referents because they are relatively accurate and publicly available. It should be noted that viscosity and density data in the NIST SUPERTRAPP is not experimental data but is calculated by the extended corresponding states model (EXCST). As mentioned In SUPERTRAPP (also called NIST4), for pure fluids the corresponding states prediction has associated uncertainties of better than 2% in compressed liquid densities and 5–8% for liquid viscosity and thermal conductivity. For mixtures, liquid densities are typically estimated to within 3% and liquid viscosity and thermal conductivity to 5–10% [38]. To clarify the comparison and ensuing discussion, the absolute relative deviation (ARD) between the MD simulation results (or the calculated results by theoretical models) and the NIST SUPERTRAPP data is used and calculated as follows.

$$ARD = \frac{\left|A^{CAL} - A^{NIST}\right|}{A^{NIST}} \times 100\% \tag{39}$$

where A^{CAL} represents the values calculated by either the MD simulation or theoretical models and A^{NIST} denotes the values from the NIST SUPERTRAPP. To allow the readers to compare to the data in this work,

all the numerical data and uncertainty estimates are provided in Supplementary Material.

3.1. Predicting viscosity using EMD simulation

In our simulations, we conducted six independent runs by changing initial velocity and the viscosity is determined by averaging over the output of six independent runs. For example, the normalized autocorrelation function (NACF) and viscosities of 1,2,4-TMB at $T = 600$ K, $P = 2$ MPa for the independent runs and their average with the correlation time are shown in Fig. 2. It can be observed that the NACFs decay relatively fast to zero in about 3000 fs.

3.2. Mixing rules

To describe the interactions between the unlike atoms, the mixing rules should be used. Here two common mixing rules for the hydrocarbon mixtures are tested: the Lorentz-Berthelot (LB) mixing rules [40] and the sixth-order mixing rules [41].

$$\varepsilon_{ij} = 2\sqrt{\varepsilon_i \varepsilon_j} \left(\frac{(\varepsilon_i)^3 \cdot (\varepsilon_j)^3}{(\varepsilon_i)^6 + (\varepsilon_j)^6} \right)$$

Sixth − order mixing rules $\tag{40}$

$$\sigma_{ij} = \left(\frac{(\sigma_i)^6 + (\sigma_j)^6}{2} \right)^{1/6}$$
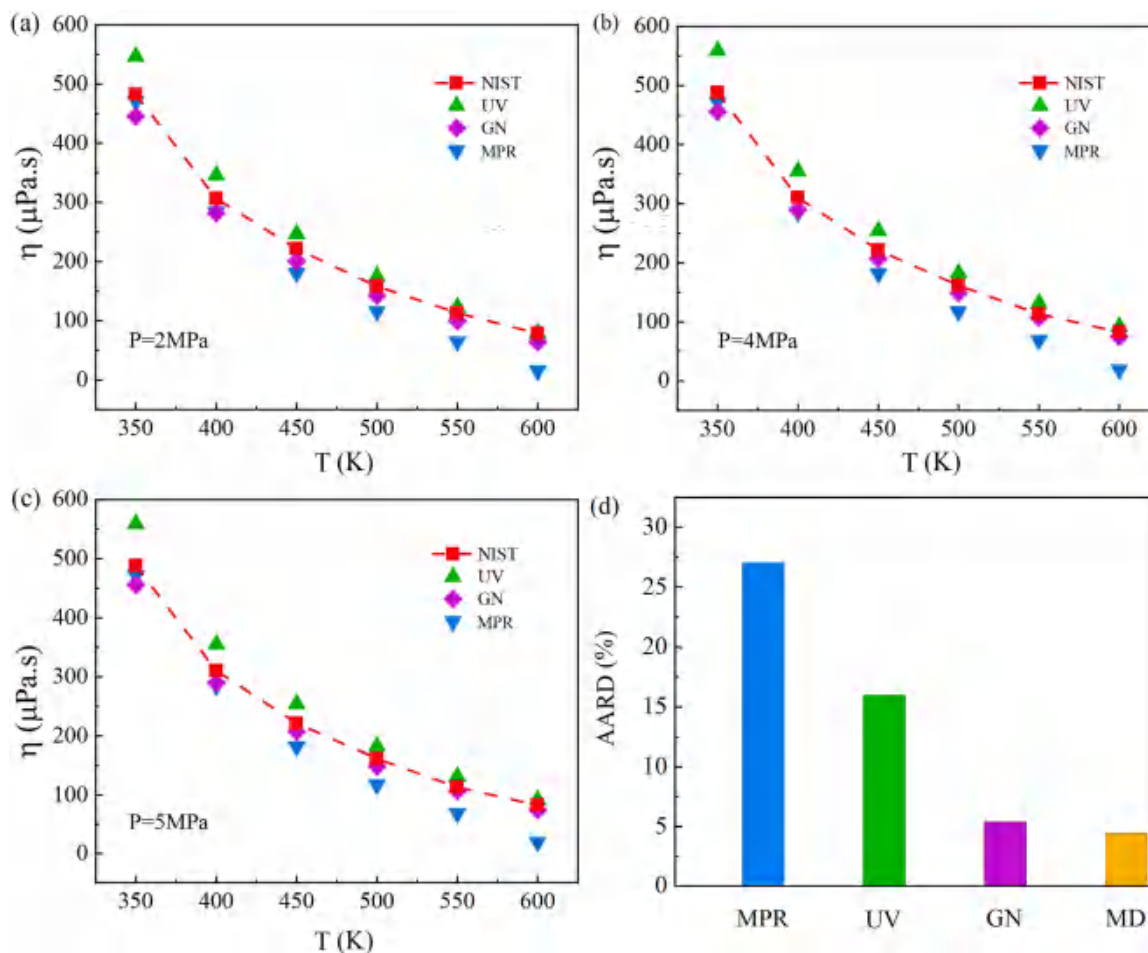
Fig. 8. Viscosity as a function of temperature calculated by theoretical models for the n-decane/1,2,4-TMB mixture under different pressures (a) 2 MPa; (b) 4 MPa; (c) 5 MPa; (d) AARDs.

$$\varepsilon_{ij} = \sqrt{\varepsilon_i \varepsilon_j}$$

LB mixing rules   (41)

$$\sigma_{ij} = \left(\frac{\sigma_i + \sigma_j}{2}\right)$$

The viscosities of n-decane are calculated using the sixth-order mixing rules at temperature of 350K-600 K and pressure of 3 MPa, and are compared with the calculation results obtained using the LB mixing rules by the authors in a previous study [16] with the same simulation strategy, as shown in Fig. 3. The corresponding NIST SUPERTRAPP data is also provided in the Figure. The results show that compared to NIST SUPERTRAPP data, the simulation results utilizing the sixth-order mixing rules produced an average absolute relative deviation (AARD) of 4.95%, whereas the LB mixing rules have AARD of 13.88%. The deviations of the prediction values produced by the sixth-order mixing rules are much smaller than those produced by the LB mixing rules, particularly at lower temperatures. This suggests that the sixth-order mixing rules for the MD simulations with the COMPASS force field can provide a better prediction accuracy than the LB mixing rules. Therefore, the sixth-order mixing rules are recommended for the LJ-9–6 potential parameters ε_{ij} and σ_{ij} to describe the interactions between the unlike atoms in the following simulations of pure 1, 2, 4-TMB and its mixture with n-decane.

3.3. Pure 1, 2, 4-TMB

The viscosities and densities for 1,2,4-TMB at different pressures are calculated via MD simulation. The results are respectively shown in Figs. 4 and 5 and are compared with the corresponding NIST

SUPERTRAPP data. The simulated viscosities and densities of 1,2,4-TMB decrease sharply with the increase in temperature and are well in agreement with the NIST SUPERTRAPP data. The summaries of the ARDs and AARDs for the viscosity and density predictions are provided in Figs. 4(d) and 5(d). The AARDs of the simulations for viscosities are 5.67%, 3.52%, and 5.38%, and for densities are 1.14%, 1.22%, and 1.05% at pressures of 2 MPa, 4 MPa, and 5 MPa, respectively.

3.4. N-decane/1,2,4-TMB binary mixture

The simulation results of viscosities and densities for the binary mixture of n-decane and 1,2,4-TMB are respectively shown in Figs. 6 and 7, and are compared with the corresponding NIST SUPERTRAPP data at different pressures. Both the simulated viscosities and the densities for the binary mixture of n-decane and 1,2,4-TMB monotonically decrease with increasing temperature. With increasing temperature, the decreasing density is due to the volume expansion, while the reasons for the decreasing viscosity may be more complicated and will be further discussed in Section 3.7. The MD simulation results have the AARDs of 4.12%, 4.65% and 4.57% for viscosity predictions and AARDs of 1.30%, 1.42% and 0.69% for density predictions at pressures of 2 MPa, 4 MPa, and 5 MPa, respectively. The overall AARDs are 4.44% for the viscosities and 1.13% for the densities. Therefore, the predicted viscosities and densities via MD simulations are in good agreement with the NIST SUPERTRAPP data. Moreover, this also indicates that the COMPASS force field with the sixth-order combining rules is suitable for the prediction of the viscosities and densities of the mixtures containing n-al-kanes and aromatics.
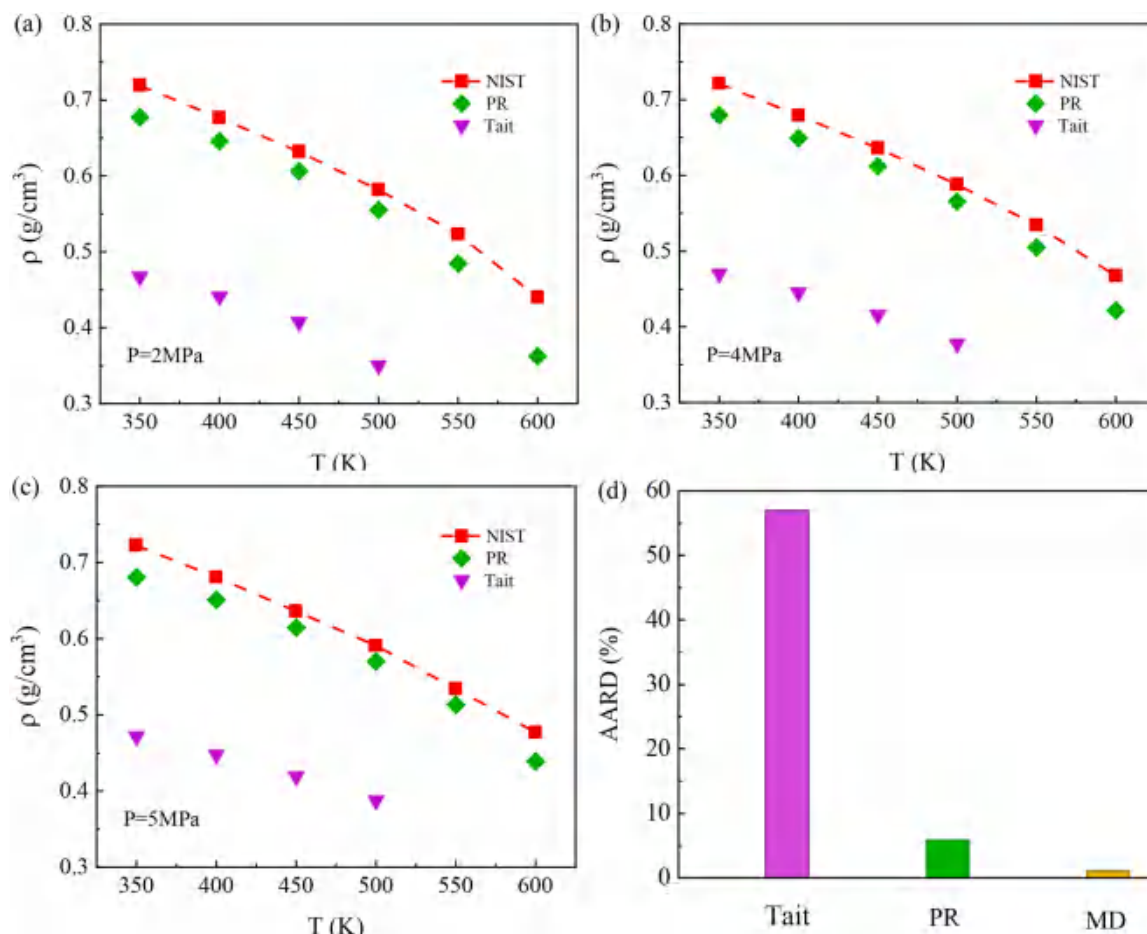
Fig. 9. Density as a function of temperature calculated by theoretical models for the n-decane/1,2,4-TMB mixture under different pressures (a) 2 MPa; (b) 4 MPa; (c) 5 MPa; (d) AARDs.

3.5. Theoretical calculation

The calculated viscosities with different theoretical models for the binary mixture of n-decane and 1,2,4-TMB are shown in Fig. 8. A summary of the AARDs of the theoretical models for viscosity prediction is also provided, as shown in Fig. 8(d). The AARDs of the calculated viscosities are 26.64%, 27.82%, and 26.52% for the MPR equation; 15.75%, 15.75%, and 16.39% for UV model; and 5.7%, 5.59%, and 4.86% for GN model at pressures of 2 MPa, 4 MPa, and 5 MPa, respectively. The overall AARDs of the viscosities are 27.01%, 15.96, and 5.38% for the MPR equation, UV model and GN model, respectively. The reason for such a relatively large deviation generated by the MPR equation may be because there is a lack of binary interaction parameters for the mixed system of n-alkanes and aromatics. Evidently, the predictive accuracy of the GN model is the best among the three theoretical models, but still slightly worse than that of the MD predictions with the superior overall AARDs of 4.44%.

Fig. 9 depicts the calculated densities by the PR equation and Tait equation for the binary mixture of n-decane and 1,2,4-TMB. The AARDs of the PR equation are 7.33%, 5.5%, and 4.8%, while the AARDs of the Tait equation are 53.1%, 53.3%, and 65.9%; these values correspond to pressures of 2 MPa, 4 MPa, and 5 MPa, respectively. The Tait equation greatly underestimates the densities of the binary mixture, which may be due to the equations having been fitted based on non-polar molecules, and hence not entirely suitable for predicting polar molecules. Fig. 9(d) compares the overall AARDs of the two theoretical models and the MD method. The overall AARDs of the PR equation and Tait equation are respectively 5.87 and 57.4%, respectively, which are larger than that

of the MD method with a value of 1.13% obtained above. Thus, it can be concluded the MD method is superior to the compared theoretical models for the prediction accuracy of the viscosity and density of the binary mixture.

3.6. Self-diffusion coefficient

Using the time-dependent mean square displacement (MSD), the self-diffusion coefficient is determined as follows:

$$D_i = \frac{1}{6N} \lim_{t \to \infty} \frac{d}{dt}(MSD) \tag{42}$$

$$MSD = \left\langle \sum_{i=1}^{N} [r_i(t) - r_i(0)]^2 \right\rangle \tag{43}$$

where D_i is the self-diffusion coefficient of pure component i; $\overrightarrow{r_i(t)}$ and $\overrightarrow{r_i(0)}$ are the vector coordinate of the center of mass of molecule i at time t and 0, respectively; $\langle \rangle$ is the average value. The self-diffusion coefficient calculated by MD simulations requires a finite-size correction (Yeh-Hummer correction) [42] which has the formula as follows.

$$D_0 = D_{PBC} + 2.837297 k_B T / (6\pi\eta L) \tag{44}$$

where D_0 is the Yeh-Hummer corrected self-diffusion coefficient, D_{PBC} is the self-diffusion coefficient calculated in the simulation, k_B is the Boltzmann constant, T is the absolute temperature and η is the shear viscosity of the solvent, L is the length of simulation cubic box. Fig. 10(a)-(c) respectively depicts the temperature dependence of the
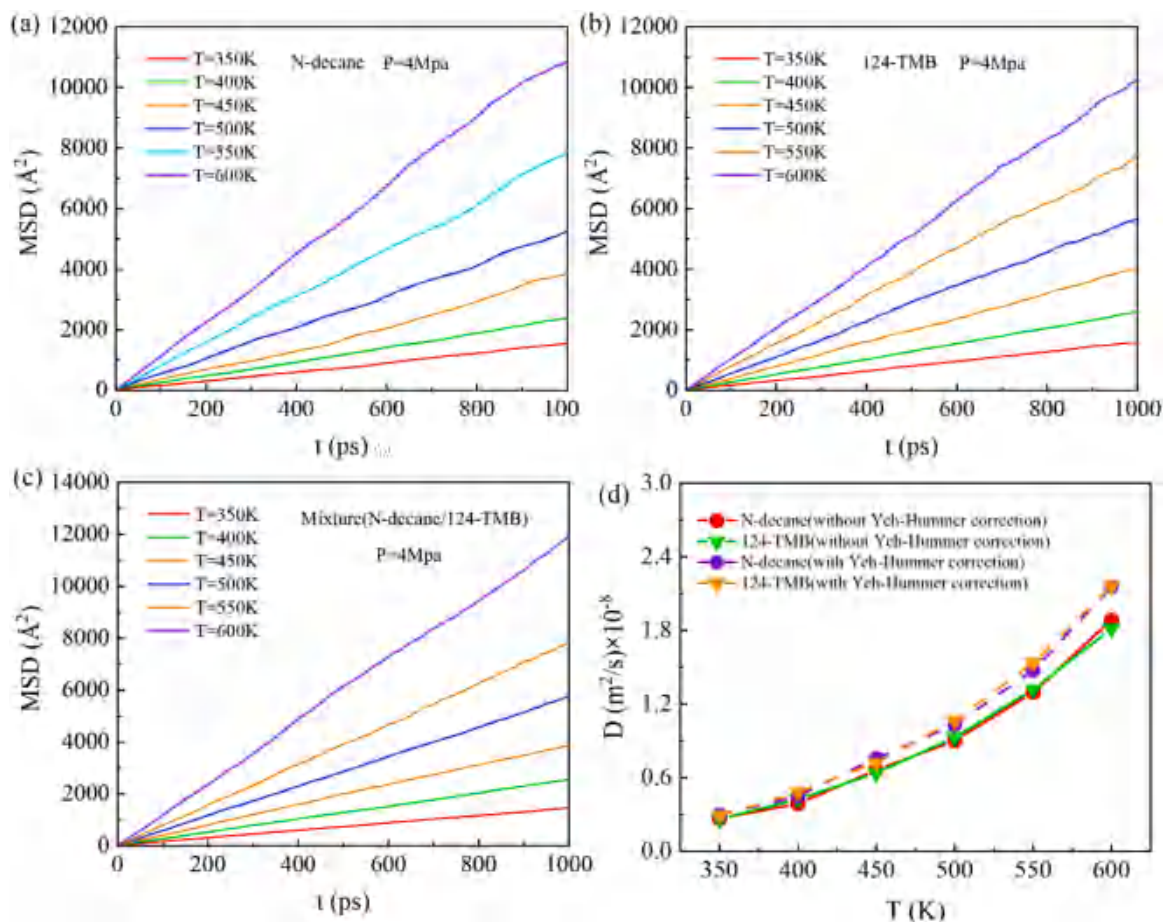
Fig. 10. The calculated MSD and the self-diffusion coefficient D: (a) MSD of n-decane in the binary mixture; (b) MSD of 1,2,4-TMB in the binary mixture; (c) MSD of the binary mixture; (d) Self-diffusion coefficient of n-decane and 1,2,4-TMB in the binary mixture.
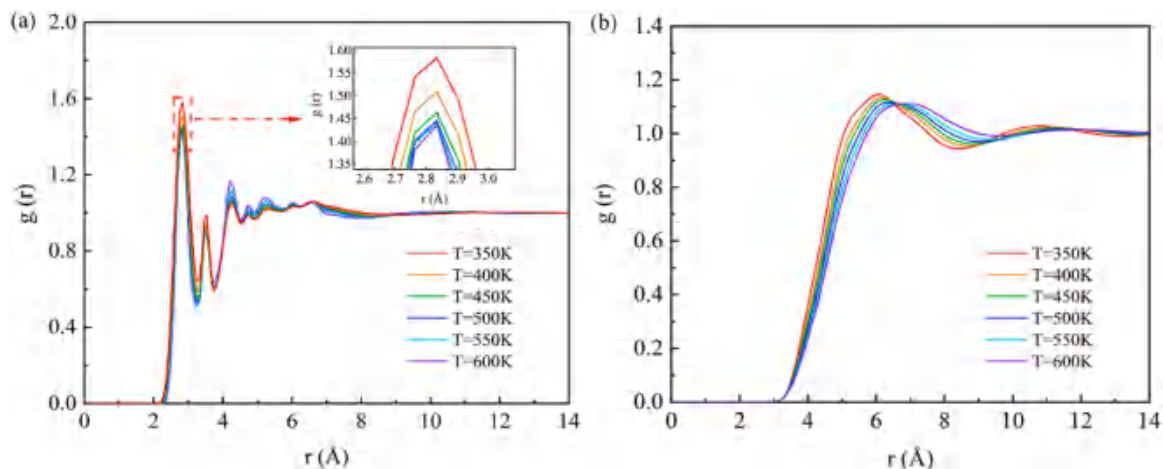
Fig. 11. The RDF as a function of temperature: (a) C_{H2}—H (b) C_{H2}—C_a.

MSDs for n-decane, 1,2,4-TMB, and their mixture, and Fig. 10(d) shows the temperature dependence of the calculated self-diffusion coefficient of n-decane and 1,2,4-TMB in the binary mixture before and after the Yeh-Hummer correction, at a pressure of 4 MPa. As shown in Fig. 10(a)-(c), the slope of MSDs for n-decane, 1,2,4-TMB, and their mixture increases with ascending temperature. To determine the time range for fitting the self-diffusion coefficient, a region with a slope closed to 1 in log (MSD) -log (t) curve is used as the effective time range [43]. From Fig. 10(d), it can be observed that the self-diffusion coefficients of

n-decane and 1,2,4-TMB in the binary mixture increase non-linearly with increasing temperature, which indicates that molecular diffusion is enhanced with temperature.

The viscosity of the system is determined by the internal friction and intermolecular attraction between molecules. As the temperature rises, the intermolecular spacing of the molecules n-decane and 1,2,4-TMB increases due to volume expansion, lowering intermolecular attraction and resulting in a decrease in viscosity. Our previous study [16] has shown that the Rouse model can describe the variation trend of
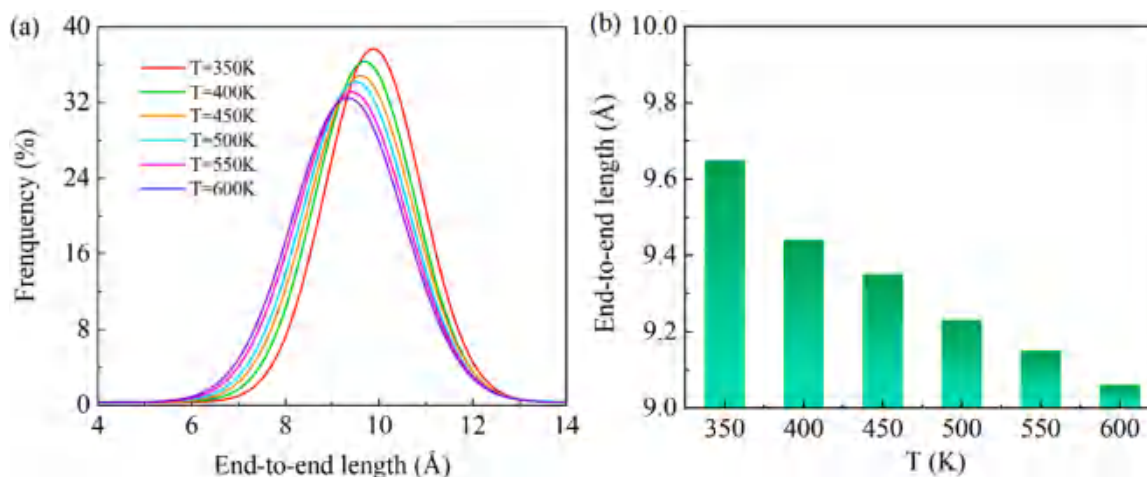
Fig. 12. End-to-end length of n-decane in the binary mixture of n-decane and 1,2,4-TMB at different temperatures: (a) end-to-end length distribution; (b) average end-to-end length.
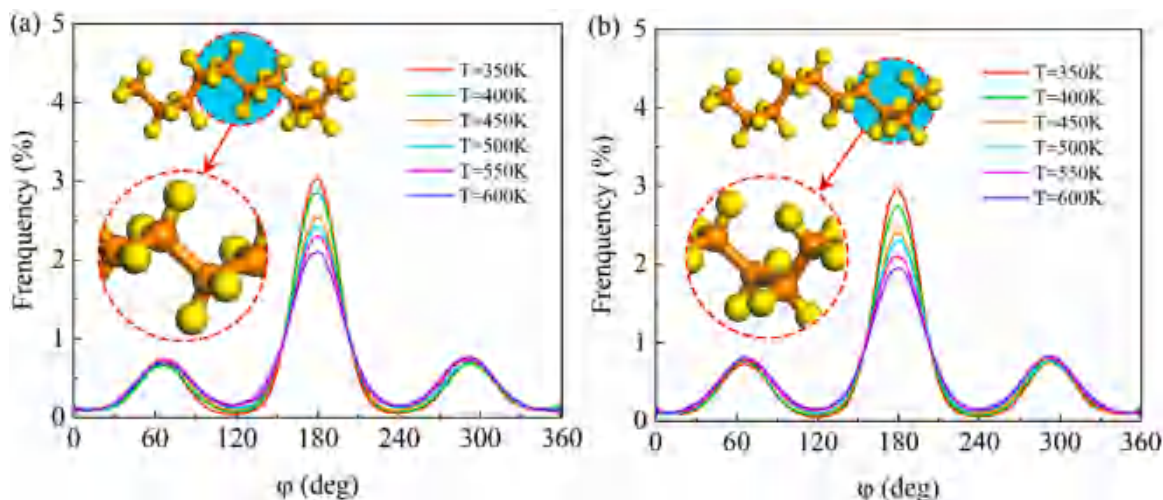
Fig. 13. Dihedral angle distribution of n-decane in mixture under different temperatures.

viscosities of n-decane, n-undecane, and n-dodecane with temperature changes, albeit with a significant degree of underestimation. In the Rouse model, $\eta \propto (1/D)$. Therefore, the increase in the self-diffusion coefficients of the n-decane and 1,2,4-TMB with temperature should be an important reason for the decreasing viscosities with increasing temperatures.

3.7. Structure analysis

3.7.1. Radial distribution function

Radial distribution function (RDF, g(r)) describes how density varies as a function of distance from a reference particle. The expression is as follows:

$$g_{\alpha\beta}(r) = \frac{1}{4\pi r^2 \rho_\beta} \left[\frac{dN_{\alpha\beta}(r)}{dr} \right] \quad (45)$$

In the formula, ρ_β is the numerical density of particles β. $N_{\alpha\beta}$ is the number of β particles in a sphere with α particles as the center and radius r. In general, the first peak of $g_{\alpha\beta}(r)$ represents the aggregation degree of atoms or molecules in the first neighborhood.

Fig. 11 shows the radial distribution function of the binary mixture containing n-decane and 1,2,4-TMB at a pressure of 4 Mpa and different temperatures. As shown in Fig. 11(a), the first peaks of $g(r)_{CH_2-H}$

correspond to approximately 2.8 Å, which is consistent with the sum of Van der Waals radii of the carbon and hydrogen atoms of 2.82 Å [44]. The magnitudes of the major peaks of $g(r)_{CH_2-H}$ and $g(r)_{CH_2-C_a}$ decrease as the temperature increases. This indicates that, with ascending temperature, distances increase between n-decane molecules and the aggregation of the molecules decreases. In Fig. 11(b), the RDFs of the C_a atoms of 1,2,4-TMB and the C_{H2} atom of n-decane are plotted. It can be observed that the locations of the first peak are shifted rightwards from 6.11 Å at $T = 350$ K to 6.97 Å at $T = 600$ K. The rightward shift of these peaks indicates that the distance between molecules of n-decane and 1,2,4-TMB gradually increases with the increase of temperature.

3.7.2. End-to-end length of n-decane in mixture

The end-to-end length and dihedral angle distribution of the n-decane molecules in the system at different temperatures are calculated. Fig. 12(a) shows the distribution function of the end-to-end length of n-decane molecules at different temperatures. It can be seen that the location of the peaks shifts to the left and the peaks values decline with increasing temperature. This means that the average end-to-end length of n-decane molecules declines with temperature. The average end-to-end length of the n-decane molecules is statistically calculated as shown in Fig. 12(b). Such a decrease in average end-to-end length of the n-decane molecules can be explained by the dihedral angle distribution

of n-decane in the mixture. Typically, the dihedral angle distribution of atom groups at the chain head and atom groups in the middle of the chain of the n-decane molecules are calculated, as shown in Fig. 13. The two smaller peaks, near 60° and 300°, are related to the two gauche conformations, while the highest peak, about 180°, represents the dihedral angles in the trans-conformation, which corresponds to the global minimum in energy [45]. It can be seen that the dominant peaks at 180° decrease monotonically with temperature. This indicates that the twist of the chain becomes more significantly with the increasing temperature, leading to a decrease in the end-to-end length of n-decane molecules.

The size of the molecules and the end-to-end length of n-decane affect the transport behavior of the system. Although the short chain of n-decane cannot satisfy the Gaussian chain, the end-to-end length of the molecular chain and the radius of gyration (R_g) are still proportional [46]. The influence of the radius of gyration on the viscosities can be described by the Rouse model, where the viscosity $\eta \propto R_g^2$. With the decrease of the end-to-end length of n-decane, the radius of gyration is decreased which should therefore contribute to the decrease of viscosity. Therefore, the decrease in the end-to-end length of the molecular chain is an important factor in decreasing viscosity.

4. Conclusion

In this work, the viscosities and densities of pure 1,2,4-TMB and its binary mixture with n-decane are investigated using MD simulations with the COMPASS force field. The simulated viscosities and densities are compared with those obtained by theoretical models: the MPR equation, GN model, and UV model for viscosity; the PR equation and the Tait equation for density. Results show that in the MD simulations with the COMPASS force field, the sixth-order combining rules demonstrate superior prediction accuracy than the LB combining rules. The MD simulation results are in agreement with the NIST SUPERTRAPP data, and the MD simulation model achieves superior performance than the theoretical models. In addition, the self-diffusion coefficient, radial distribution function, end-to-end length, and dihedral angle distribution of n-decane in the binary mixture are analyzed. It is found that the decreased end-to-end length due to the twist of the n-decane chains is an important factor impacting the decrease of viscosity with increasing temperature. This study provides a good reference for the simulation and prediction of the thermophysical properties of mixtures containing n-alkanes and aromatics.

CRediT authorship contribution statement

Xueming Yang: Conceptualization, Methodology, Validation, Writing – original draft. **Qiang Liu:** Investigation, Writing – review & editing. **Xiaozhong Zhang:** Visualization, Validation. **Chang Ji:** Writing – review & editing, Validation. **Bingyang Cao:** Supervision, Software.

Declaration of Competing Interest

The authors declare that they have no known competing financial interests or personal relationships that could have appeared to influence the work reported in this paper.

Data Availability

I have shared my data in the attached Supplementary material.

Acknowledgments

Supplementary materials

Supplementary material associated with this article can be found, in the online version, at doi:10.1016/j.fluid.2022.113566.

References

[1] Y. Shen, Y. Liu, B. Cao, C4+ surrogate models for thermophysical properties of aviation kerosene RP-3 at supercritical pressures, Energy Fuels 35 (2021) 7858–7865, https://doi.org/10.1021/acs.energyfuels.1c00326.

[2] Y. Mao, L. Yu, Y. Qian, S. Wang, Z. Wu, M. Raza, L. Zhu, X. Hu, X. Lu, Development and validation of a detailed kinetic model for RP-3 aviation fuel based on a surrogate formulated by emulating macroscopic properties and microscopic structure, Combust. Flame 229 (2021), 111401, https://doi.org/10.1016/j.combustflame.2021.111401.

[3] W. Liu, X. Liang, B. Lin, H. Lin, Z. Huang, D. Han, A comparative study on soot particle size distributions in premixed flames of RP-3 jet fuel and its surrogates, Fuel 259 (2020), 116222, https://doi.org/10.1016/j.fuel.2019.116222.

[4] C. Zhang, B. Li, F. Rao, P. Li, X. Li, A shock tube study of the autoignition characteristics of RP-3 jet fuel, Proc. Combust. Instit. 35 (2015) 3151–3158, https://doi.org/10.1016/j.proci.2014.05.017.

[5] S. Aminane, M. Sicard, F. Ser, L. Sicard, Experimental study of the autoxidation of n-dodecane and 1, 2, 4-trimethylbenzene, in: IASH (2019) 2019.

[6] J. Xu, J. Guo, A. Liu, J. Wang, N. Tan, X. Li, Construction of autoignition mechanisms for the combustion of RP-3 surrogate fuel and kinetics simulation, Acta Phys. Chim. Sin. 31 (2015) 643–652, https://doi.org/10.3866/PKU.WHXB201503022.

[7] G. Zhao, Z. Yuan, J. Yin, S. Ma, Experimental Investigation of the thermophysical properties of the bio-aviation fuel surrogates: binary and ternary mixtures of n-dodecane, methyl butyrate, and methyl decanoate, J. Chem. Eng. Data 64 (2019) 5510–5522, https://doi.org/10.1021/acs.jced.9b00643.

[8] J. Deng, Y. Yang, P. Wang, G. Ouyang, Z. Huang, Excess Molar Volumes and Surface Tensions of Trimethylbenzene + Ethylene Glycol Ester at 298.15K and 313.15K, J. Chem. Eng. Data 51 (2006) 725–729, https://doi.org/10.1021/je050484k.

[9] Y. Duan, W. Liu, X. Liang, D. Han, Effects of branch structure of alkylbenzenes on spray auto-ignition of n-decane and alkylbenzenes blends, Int. J. Engine Res. 22 (2020) 1636–1651, https://doi.org/10.1177/1468087420914716.

[10] Y. Duan, W. Liu, Z. Huang, D. Han, An experimental study on spray auto-ignition of RP-3 jet fuel and its surrogates, Front. Energy 15 (2021) 396–404, https://doi.org/10.1007/s11708-020-0715-y.

[11] D.L. Prak, B.H. Morrow, J.S. Cowart, J.A. Harrison, Binary Mixtures of Aromatic Compounds (n-Propylbenzene, 1,3,5-Trimethylbenzene, and 1,2,4-Trimethylbenzene) with 2,2,4,6,6-Pentamethylheptane: densities, Viscosities, Speeds of Sound, Bulk Moduli, Surface Tensions, and Flash Points at 0.1MPa, J. Chem. Eng. Data 65 (2020) 2625–2641, https://doi.org/10.1021/acs.jced.0c00020.

[12] S. Rabet, G. Raabe, Comparison of the GAFF, OPLSAA and CHARMM27 force field for the reproduction of the thermodynamics properties of furfural, 2-methylfuran, 2,5-dimethylfuran and 5-hydroxymethylfurfural, Fluid Phase Equilib. 554 (2022), 113331, https://doi.org/10.1016/j.fluid.2021.113331.

[13] A.W.S. Hamani, J.-.P. Bazile, H. Hoang, H.T. Luc, J.-.L. Daridon, G. Galliero, Thermophysical properties of simple molecular liquid mixtures: on the limitations of some force fields, J. Mol. Liq. 303 (2020), 112663, https://doi.org/10.1016/j.molliq.2020.112663.

[14] X. Yang, Y. Gao, M. Zhang, W. Jiang, B. Cao, Comparison of atomic simulation methods for computing thermal conductivity of n-decane at sub/supercritical pressure, J. Mol. Liq. 342 (2021), 117478, https://doi.org/10.1016/j.molliq.2021.117478.

[15] D.K. Dysthe, A.H. Fuchs, B. Rousseau, Fluid transport properties by equilibrium molecular dynamics. III. Evaluation of united atom interaction potential models for pure alkanes, J. Chem. Phys. 112 (2000) 7581–7590, https://doi.org/10.1063/1.481353.

[16] X. Yang, M. Zhang, Y. Gao, J. Cui, B. Cao, Molecular dynamics study on viscosities of sub/supercritical n-decane, n-undecane and n-dodecane, J. Mol. Liq. 335 (2021), 116180, https://doi.org/10.1016/j.molliq.2021.116180.

[17] H.K. Chilukoti, G. Kikugawa, T. Ohara, A molecular dynamics study on transport properties and structure at the liquid–vapor interfaces of alkanes, Int. J. Heat Mass Transfer. 59 (2013) 144–154, https://doi.org/10.1016/j.ijheatmasstransfer.2012.12.015.

[18] R.S. Payal, S. Balasubramanian, I. Rudra, K. Tandon, I. Mahlke, D. Doyle, R. Cracknell, Shear viscosity of linear alkanes through molecular simulations: quantitative tests for n-decane and n-hexadecane, Mol. Simul. 38 (2012) 1234–1241, https://doi.org/10.1080/08927022.2012.702423.

[19] N.D. Kondratyuk, V.V. Pisarev, Predicting shear viscosity of 1,1-diphenylethane at high pressures by molecular dynamics methods, Fluid Phase Equilib. 544 (545) (2021), 113100, https://doi.org/10.1016/j.fluid.2021.113100.

[20] X. Nie, Z. Du, L. Zhao, S. Deng, Y. Zhang, Molecular dynamics study on transport properties of supercritical working fluids: literature review and case study, Appl. Energy 250 (2019) 63–80, https://doi.org/10.1016/j.apenergy.2019.04.156.

[21] K.D. Papavasileiou, L.D. Peristeras, A. Bick, I.G. Economou, Molecular dynamics simulation of pure n-alkanes and their mixtures at elevated temperatures using atomistic and coarse-grained force fields, J. Phys. Chem. B 123 (2019) 6229–6243, https://doi.org/10.1021/acs.jpcb.9b02840.

[22] H. Sun, COMPASS: an ab initio force-field optimized for condensed-phase applications overview with details on alkane and benzene compounds, J. Phys. Chem. B 102 (1998) 7338–7364, https://doi.org/10.1021/jp980939v.

[23] C.S.T. Cui, P.T. Cummings, H. D, The calculation of viscosity of liquid n-decane and n-hexadecane by the Green-Kubo method, Mol Phys 93 (1998) 117–122, https://doi.org/10.1080/002689798169500.

[24] S. Plimpton, Fast parallel algorithms for short-range molecular dynamics, J. Comput. Phys. 117 (1995) 1–19, https://doi.org/10.1006/jcph.1995.1039.

[25] C. Chen, X. Jiang, Y. Sui, Prediction of transport properties of fuels in supercritical conditions by molecular dynamics simulation, Energy Procedia 158 (2019) 1700–1705, https://doi.org/10.1016/j.egypro.2019.01.396.

[26] R. Lin, J. Tao, Q. Liu, X. Zhang, B. Cao, Molecular dynamics simulation of thermophysical properties of binary RP-3 surrogate fuel mixtures containing trimethylbenzene, n-decane, and n-dodecane, J Mol Liq (2022), 119258, https://doi.org/10.1016/j.molliq.2022.119258.

[27] X. Yang, J. Xu, S. Wu, M. Yu, B. Hu, B. Cao, J. Li, A molecular dynamics simulation study of PVT properties for H2O/H2/CO2 mixtures in near-critical and supercritical regions of water, Int. J. Hydrogen Energy 43 (2018) 10980–10990, https://doi.org/10.1016/j.ijhydene.2018.04.214.

[28] X.Q. Guo, C.Y. Sun, S.X. Rong, G.J. Chen, T.M. Guo, Equation of state analog correlations for the viscosity and thermal conductivity of hydrocarbons and reservoir fluids, J. Pet. Sci. Eng. 30 (2001) 15–27, https://doi.org/10.1016/S0920-4105(01)00098-5.

[29] A.K. Mishra, A. Kumar, Modified Guo viscosity model for heavier hydrocarbon components and their mixtures, J. Pet. Sci. Eng. 182 (2019), 106248, https://doi.org/10.1016/j.petrol.2019.106248.

[30] W. Marczak, N. Adamczyk, M. Łężniak, Viscosity of associated mixtures approximated by the Grunberg-Nissan model, Int. J. Thermophys. 33 (2011) 680–691, https://doi.org/10.1007/s10765-011-1100-1.

[31] Y. Gaston-Bonhomme, P. Petrino, J.L. Chevalier, UNIFAC—VISCO group contribution method for predicting kinematic viscosity: extension and temperature dependence, Chem. Eng. Sci. 49 (1994) 1799–1806, https://doi.org/10.1016/0009-2509(94)80065-0.

[32] W. Marczak, N. Adamczyk, M. Łężniak, Viscosity of associated mixtures approximated by the Grunberg-Nissan model, Int. J. Thermophys. 33 (2012) 680–691, https://doi.org/10.1007/s10765-011-1100-1.

[33] D.M. Bajić, E.M. Živković, S.P. Šerbanović, M.L. Kijevčanin, Experimental measurements and modelling of volumetric properties, refractive index and viscosity of selected binary systems with butyl lactate at 288.15–323.15K and atmospheric pressure. New UNIFAC-VISCO interaction parameters, Thermochim Acta 562 (2013) 42–55, https://doi.org/10.1016/j.tca.2013.03.025.

[34] A.M. Abudour, S.A. Mohammad, R.L. Robinson, K.A.M. Gasem, Volume-translated Peng-Robinson equation of state for liquid densities of diverse binary mixtures, Fluid Phase Equilib 349 (2013) 37–55, https://doi.org/10.1016/j.fluid.2013.04.002.

[35] M. Aalto, K.I. Keskinen, J. Aittamaa, S. Liukkonen, An improved correlation for compressed liquid densities of hydrocarbons. Part 2. Mixtures, Fluid Phase Equilib. 114 (1996) 21–35, https://doi.org/10.1016/0378-3812(95)02824-2.

[36] M.L. Huber, NIST Thermophysical properties of hydrocarbon mixtures database (SUPERTRAPP), version 3.2, (2007).

[37] F.R. Hauck, Z. Yang, S.T. Kosir, J.S. Heyne, A. Landera, A. George, Experimental Validation of Viscosity Blending Rules and Extrapolation for Sustainable Aviation Fuel, in: AIAA Propulsion and Energy 2020 Forum (2020), https://doi.org/10.2514/6.2020-3671.

[38] M. Huber, D. Friend, E. Lemmon, 2022 Thermophysical property computer packages from nist of interest to the natural gass industry.

[39] R. Lin, L.L. Tavlarides, Thermophysical properties needed for the development of the supercritical diesel combustion technology: evaluation of diesel fuel surrogate models, J Supercrit Fluids 71 (2012) 136–146, https://doi.org/10.1016/j.supflu.2012.08.003.

[40] M. Allen, D. Tildesley, Computer Simulation of Liquids, Oxford university press, 1989 [Google Scholar].

[41] M. Waldman, A.T. Hagler, New combining rules for rare gas van der waals parameters, J. Comput. Chem. 14 (1993) 1077–1084, https://doi.org/10.1002/jcc.540140909.

[42] I.-C. Yeh, G. Hummer, System-size dependence of diffusion coefficients and viscosities from molecular dynamics simulations with periodic boundary conditions, J. Phys. Chem. B 108 (2004) 15873–15879, https://doi.org/10.1021/jp0477147.

[43] X. Wang, L. Sun, X. Zhang, S. Zhang, J. Wang, Y. Zhang, The effect of nanoparticles on the microstructure of alkanes: a molecular dynamics study, J. Mol. Liq. 309 (2020), 113162, https://doi.org/10.1016/j.molliq.2020.113162.

[44] Y.V. Zefirov, P.M. Zorky, New applications of van der Waals radii in chemistry, Russ. Chem. Rev. 64 (1995) 415–428, https://doi.org/10.1070/rc1995v064n05abeh000157.

[45] D.A. Bernard-Brunel, J.J. Potoff, Effect of torsional potential on the predicted phase behavior of n-alkanes, Fluid Phase Equilib. 279 (2009) 100–104, https://doi.org/10.1016/j.fluid.2009.02.008.

[46] M. Mondello, G.S. Grest, E.B. Webb III, P. Peczak, Dynamics of n-alkanes: comparison to Rouse model, J. Chem. Phys. 109 (1998) 798–805, https://doi.org/10.1063/1.476619.